Understanding the Persistence of Sea Surface Temperature Anomalies in Midlatitudes

CLARA DESER

National Center for Atmospheric Research, Boulder, Colorado

MICHAEL A. ALEXANDER AND MICHAEL S. TIMLIN

Climate Diagnostics Center, Boulder, Colorado

(Manuscript received 21 December 2001, in final form 16 July 2002)

ABSTRACT

An extension of the simple stochastic climate model of Frankignoul and Hasselman that includes the effects of seasonal variations in upper-ocean mixed layer depth upon the persistence of winter sea surface temperature (SST) anomalies is proposed. Seasonal variations in mixed layer depth allow for the ''reemergence mechanism,'' whereby thermal anomalies stored in the deep winter mixed layer persist at depth through summer and become partially reentrained into the mixed layer during the following winter. In this way, SST anomalies can recur from winter to winter without persisting through the intervening summer. Reformulating the simple stochastic climate model in terms of an *effective* ocean thermal capacity given by the depth of the winter mixed layer, thereby implicitly taking into account reemergence, is shown to provide a favorable fit to the observed winter-to-winter SST autocorrelations in the North Atlantic and Pacific, and represents a considerable improvement over the original model. The extended model also compares favorably with results from an entraining bulk ocean mixed layer model coupled to an atmospheric general circulation model. The authors propose that the extended model be adopted as the new ''null hypothesis'' for interannual SST variability in middle and high latitudes.

1. Introduction

The oceans are generally regarded as the ''flywheel'' of the climate system, providing a vast source of thermal inertia to the overlying atmosphere. The large thermal inertia of the oceans derives from their heat storage capacity: ~2.5 m of water contains as much energy as an entire atmospheric column. The ocean communicates its thermal inertia to the atmosphere largely via the surface turbulent fluxes of sensible and latent energy. These turbulent fluxes, in turn, depend upon a single oceanic variable, the sea surface temperature (SST), and several atmospheric parameters including the near-surface wind speed, air temperature, and relative humidity. Given the primary importance of SST in the thermal communication between the ocean and atmosphere, and the potential for SST variations to induce slow climatic fluctuations, it is of interest to investigate the nature of temporal persistence of large-scale SST anomalies. In the present study, we focus on understanding the behavior of SST anomaly persistence in middle and high latitudes.

Large-scale SST anomaly persistence in the North Atlantic and Pacific has been examined in numerous studies, including Namias and Born (1970, 1974), Reynolds (1978), Frankignoul and Reynolds (1983), Namias et al. (1988), Bhatt et al. (1998), Watanabe and Kimoto (2000), Kushnir et al. (2002), and Timlin et al. (2002). Collectively these studies indicate typical SST *e*-folding timescales on the order of 3–6 months based on data from all calendar months. However, as recognized by Namias and Born, the duration of large-scale SST anomalies is seasonally dependent. Specifically, Namias and Born noted a tendency for SST anomalies at selected locations in the North Atlantic and Pacific to recur from one winter to the next without persisting through the intervening summer, effectively extending the memory of winter SST anomalies to longer than 1 yr. In contrast, summer SST anomalies decay rapidly, within a couple of months, at the locations examined by Namias and Born. Subsequent studies, including Namias et al. (1988), Bhatt et al. 1998, Watanabe and Kimoto (2000), Kushnir et al. (2002), and Timlin et al. (2002), have confirmed the strong seasonal dependence of the persistence characteristics of large-scale SST anomaly patterns in both the North Atlantic and North Pacific.

What physical processes contribute to the seasonal differences in persistence of extratropical SST anomalies? Namias and Born speculated that the seasonal evolution of upper-ocean mixed layer depth was a crucial factor. They hypothesized that vigorous air–sea energy

Corresponding author address: Dr. Clara Deser, Climate and Global Dynamics Division, NCAR, P.O. Box 3000, Boulder, CO 80307.
E-mail: cdeser@ucar.edu

© 2003 American Meteorological Society

exchange during winter creates temperature perturbations that extend down to the base of the deep winter mixed layer, typically 100–200 m in the North Pacific and considerably deeper in portions of the North Atlantic. When the mixed layer shoals (or more accurately, reforms) in late spring, the winter thermal anomalies become sequestered beneath the shallow (~20–30 m) summer mixed layer in a highly stratified environment (the seasonal thermocline) and become effectively insulated from further air–sea heat exchange. As the mixed layer deepens again in late fall and early winter, a portion of the subsurface thermal anomalies may become reentrained into the mixed layer, thus influencing the mixed layer heat budget and SST in the following winter. In this way, an SST anomaly would recur from one winter to the next without persisting through the intervening summer. Alexander and Deser (1995) termed this process the reemergence mechanism.

This scenario was tested in a series of studies examining the vertical structure of upper-ocean temperature anomalies that accompany reemerging winter SST anomalies. Alexander and Deser (1995) used upper-ocean temperature profiles from ocean weather ships in the North Atlantic and Pacific to document that winter mixed layer temperature anomalies persist beneath the shallow summer mixed layer, and that a portion of the anomalous heat storage is reentrained into the mixed layer during the following early winter, imparting a signal to the following winter's SST anomaly. In a follow-up study, Alexander et al. (1999) used gridded subsurface temperature profiles over the North Pacific to document the spatial extent of the reemergence process, and to investigate the seasonal dependence of the signal. It was clear from that study that reemergence occurs basinwide, but that the timing can differ considerably from one region to the next due to differences in the depth of the winter mixed layer. Also, an SST anomaly formed in late winter (March) when the mixed layer is deepest will reemerge later than one formed in early summer (June) when the mixed layer is shallower. Thus, SST anomalies from January through June all exhibit reemergence during the following winter, but the timing of when they are reentrained into the mixed layer is dependent upon the depth of the mixed layer when they were originally formed. Recently, Watanabe and Kimoto (2000) and Timlin et al. (2002) have analyzed gridded subsurface temperature profiles in the North Atlantic to document the reemergence process there, and showed that the larger the difference between the depth of the mixed layer in summer and winter, the stronger the influence of the reemergence process upon winter SST anomalies.

In this study, we shall make extensive use of the concept of the reemergence mechanism to understand the nature of SST anomaly persistence over the North Atlantic and Pacific. We focus on the following question: to what extent can ocean mixed layer processes account for the observed seasonal and geographical dependence of SST anomaly persistence? To address this question, we introduce a conceptual physical framework based upon the paradigm of the simple stochastic climate model for midlatitude SST variability due to Frankignoul and Hasselmann (1977, hereafter FH77). We consider first the simplest possible coupled ocean–atmosphere system consisting of a slab ocean mixed layer of fixed depth H coupled to an atmosphere above and an ocean interior below (Fig. 1, left), the original formulation of FH77. Conceptually, this model assumes that ocean mixed layer temperature anomalies T' are forced by random atmospheric variability (with a short decorrelation time, on the order of a week or two) and decay by damping back to the atmosphere (modeled as a negative linear feedback term): dynamical processes in the ocean interior do not impact T'. This model yields typical e-folding timescales for SST anomalies on the order of 3–6 months depending upon the value used for H (the deeper the mixed layer, the larger the associated thermal inertia, which is manifest as a longer persistence time). This paradigm has been used successfully to understand the initial rate of decay of SST anomalies in the North Pacific and Atlantic (cf. FH77; Reynolds 1978; Frankignoul and Reynolds 1983; Herterich and Hasselmann 1987; Lau and Nath 1996; Alexander and Penland 1996; Hall and Manabe 1997; Deser and Timlin 1997). However, this framework does not explain the high winter-to-winter memory of SST anomalies documented in the studies cited earlier. To account for winter-to-winter persistence, we propose the following extension to the FH77 paradigm.

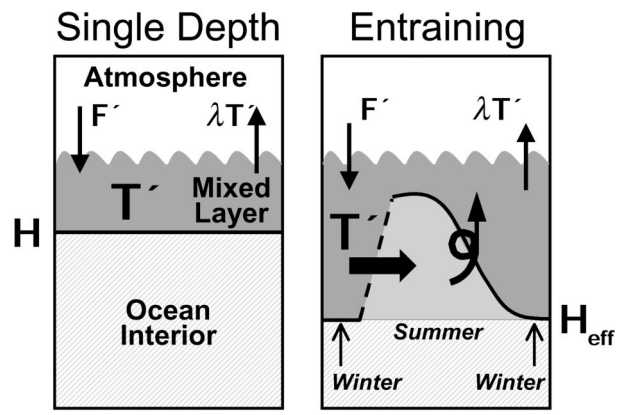

FIG. 1. Conceptual ocean–atmosphere systems considered in this study. (left) The original simple stochastic climate model of Frankignoul and Hasselmann (1977) and (right) the proposed extension. In both systems, temperature anomalies (T') in the ocean mixed layer are assumed to result from atmospheric forcing (F') only and damp back to the atmosphere at a rate $\lambda T'$. In the original model, the mixed layer depth (H) is constant; in the extended model, H undergoes a strong seasonal cycle, with largest extent in winter and smallest in summer. In this configuration, T' created in winter can persist beneath the summer mixed layer and become reentrained into the mixed layer the following winter, as indicated schematically by the thick black arrows. The effective thermal capacity of this system depends upon the depth of the winter mixed layer (H_{eff}).

As discussed earlier, the reemergence mechanism depends on the existence of a strong seasonal cycle in mixed layer depth, typical of middle and high latitudes. Extending the mixed layer ocean–atmosphere system to include a seasonally varying H (Fig. 1, right) allows for reemergence by incorporating the entrainment/detrainment process. In this new system, thermal anomalies created by wintertime atmospheric forcing persist at depth through summer and become reentrained into the mixed layer during the following late fall and early winter, as indicated schematically by the arrows in Fig. 1 (right). In the absence of additional oceanic processes, for example, turbulent mixing, diffusion, and subduction through the main thermocline, and advection by geostrophic and thermohaline currents, this system may be viewed in a manner analogous to the simple stochastic climate model where the mixed layer depth H is reinterpreted as an ''effective'' depth H (hereafter denoted by H_{eff} given by the maximum mixed layer depth during the course of the seasonal cycle (typically in February or March for the northern oceans). In this view, the impact of entrainment and the reemergence mechanism upon winter SST anomaly persistence is implicitly accounted for.

We shall make use of the extended simple stochastic climate model depicted in Fig. 1 (right) to guide our analysis and physical interpretation of SST anomaly persistence in the North Pacific and Atlantic. The paper is organized as follows. The datasets and methods are described in section 2. Observational results and their physical interpretation within the framework of the extended simple stochastic climate model are presented in section 3. More sophisticated physical models are considered in section 4, including one in which an entrainment term is explicitly included within the simple stochastic climate framework, and one in which a variable-depth bulk ocean mixed layer model is coupled to an atmospheric general circulation model. Additional results are presented in section 5. The paper concludes with a discussion in section 6.

2. Data and Methods

a. SST

Monthly SST data for the period 1948–97 are obtained from the Comprehensive Ocean–Atmosphere Data Set (COADS; Woodruff et al. 1987) and the Global Sea Ice Sea Surface Temperature (GISST) dataset (version 2.3b; Raynor et al. 1996). The COADS data, binned on a $2° \times 2°$ latitude–longitude grid, are quality controlled but not smoothed in space or time, and missing data have not been filled in. The GISST data, on a $1° \times 1°$ grid, are quality controlled, smoothed in space, and missing grid boxes are filled in using an EOF-based technique. We use COADS for the regionally averaged analyses in section 3a (GISST yields virtually identical results, not shown), and GISST for the basinwide analyses in section 3c [an updated version of GISST, the Hadley Centre Sea Ice and SST (HADISST) dataset, is used in section 5a].

b. Subsurface temperature

Monthly subsurface temperature data are obtained from the Joint Environmental Data Analysis Center at the Scripps Institution of Oceanography. This archive contains temperatures at 11 levels (0, 20, 40, 60, 80, 120, 160, 200, 240, 300, and 400 m) during 1955–95. The temperature profiles, collected from mechanical and expendable bathythermographs and Nansen bottle casts, were subjected to a statistical optimal interpolation scheme to generate gridded values ($2° \times 5°$ lat–lon grid) from sparse data as described in White (1995). We make use of data during 1960–92 when the number of observations is greatest. It is worth noting that there are approximately an order of magnitude fewer upper-ocean temperature profiles than SST measurements in the surface marine archives.

In the course of this study, we noted a suspicious jump in the temperature fields at 300- and 400-m depth in the northern North Atlantic compared to shallower levels. We have therefore omitted these data from our empirical orthogonal function analysis of upper-ocean heat content over the North Atlantic (section 3a). For the regional analysis of heat content in the northern North Atlantic (section 3c), we make use of an alternative dataset provided by M. Watanabe (2000, personal communication) that extends to 500-m depth without evidence of spurious jumps (note that we only have access to the regionally averaged temperature profiles, not the full lat–lon gridded dataset). These data are based upon objective analysis using a three-dimensional variational algorithm (Derber and Rosati 1989) of subsurface temperature data from the *World Ocean Atlas 1994* (Levitus and Boyer 1994). Analyses of the gridded version of these data are presented in Watanabe and Kimoto (2000). The region we examine corresponds to the ''HIGH'' area in Watanabe and Kimoto's study.

c. Mixed layer depth

We use climatological monthly mean mixed layer depths (MLD) from Monterey and Levitus (1997) on a $1° \times 1°$ lat–lon grid, where mixed layer depth is defined as the shallowest depth where the density exceeds the surface density by 0.0125 kg m^{-3}.

d. Surface fluxes and Ekman currents

Monthly surface turbulent fluxes of sensible and latent energy were obtained from the COADS archive for the period 1948–97, using a constant exchange coefficient (1.3×10^{-3}), air density (1.2 kg m^{-3}), and specific heat of air (1004 J K^{-1} kg^{-1}). Monthly Ekman currents were computed using wind stress measurements from

COADS, and a constant drag coefficient (1.3×10^{-3}), water density (1000 kg m^{-3}) and specific heat of water (4218 J K^{-1} kg^{-1}).

e. Methods

Monthly anomalies were formed by subtracting the long-term monthly means from the appropriate month for each year. EOF analysis is based upon the area-weighted covariance matrix of monthly anomalies.

3. Results

a. Basinwide analyses of monthly heat content and SST anomalies

Guided by the physical framework of the extended simple stochastic climate model (Fig. 1, right), we examine the persistence characteristics of heat content (HC) anomalies, where HC is defined as the vertically integrated temperature anomaly from the sea surface to H_{eff} *in all months.* Thus, we do not restrict the heat content to the base of the seasonally varying mixed layer, but to the base of the deepest winter mixed layer, thus incorporating the subsurface thermal pathway indicated schematically in Fig. 1 (right). The value H_{eff} is obtained from the climatological distribution of February/March average mixed layer depths from Monterey and Levitus (1997) as shown in Fig. 2 (top). The leading EOF of monthly HC anomalies over the North Atlantic, shown in Fig. 2 (bottom), accounts for 23% of the total variance over the domain. It exhibits a primary center of action between 45° and 60°N with maximum amplitude south of Greenland, and another center of opposite polarity to the southwest near 30°N. This pattern describes an out-of-phase fluctuation between HC anomalies in the two regions, and is similar to the leading EOF of monthly SST anomalies (not shown, but see Kushnir et al. 2002 and Timlin et al. 2002) but with more weight in the northern center of action compared to the southern one. This change in spatial emphasis between the SST and HC EOF patterns is consistent with the fact that H_{eff} increases to the north (Fig. 2, top).

To quantify the temporal persistence of the HC EOF pattern, we have computed the monthly lag autocorrelation curve of the associated principal component (PC) time series based on a starting month of March [e.g., correlating the PC time series in March with the PC time series in April of the same year (year 0), May of the same year . . . January of the next year (year 1) . . . December of the year following year 1 (year 2)]. The PC time series is obtained by projecting the individual monthly HC anomaly maps upon the EOF pattern using linear regression. The HC autocorrelation curve (Fig. 3, top) decays in a relatively monotonic fashion, with values ~0.6 in year 1 and ~0.4 in year 2. The most rapid decline occurs in early winter (November–January) when the rate of mixed layer deepening is greatest, consistent with the effect of entrainment, which mixes the existing heat content anomaly with thermal anomalies newly created by the atmosphere. In contrast, the autocorrelation curve for the associated SST time series (Fig. 3, top), formed by projecting individual monthly SST anomaly maps upon the HC EOF pattern using linear regression, exhibits a pronounced seasonal cycle, with relative minima in the summers (~0.2 in year 0 and year 1, and ~0.1 in year 2) and relative maxima in the winters (~0.6 in year 1 and ~0.4 in year 2). Note that HC autocorrelations are similar to those for *winter* SST, consistent with the fact that winter SST anomalies extend to H_{eff}. Note also that the summer minima in the SST autocorrelation curve are entirely absent from the HC curve. These characteristics of the HC and SST autocorrelation functions are qualitatively consistent with our simple conceptual model of a seasonally varying mixed layer that includes entrainment and the subsurface thermal pathway from winter to winter. The corresponding *e*-folding timescale for HC anomalies or, equivalently, winter SST anomalies is ~2–3 yr. None of the autocorrelation curves change appreciably when the data are first linearly detrended (not shown).

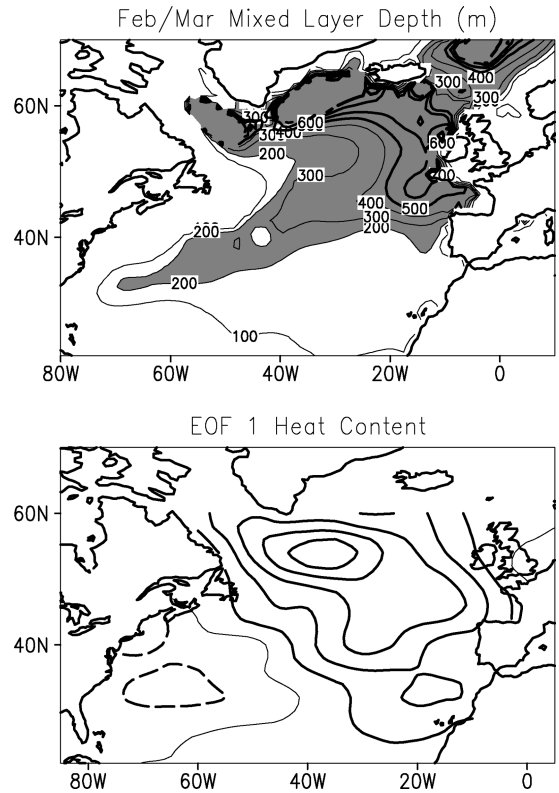

FIG. 2. (top) Observed long-term mean winter mixed layer depths in the North Atlantic (values > 200 m shaded). (bottom) Leading EOF of monthly heat content anomalies in the North Atlantic during 1960–92. Thick solid (dashed) contours indicate positive (negative) values; the contour interval is arbitrary.

When all months of the year are used to construct the SST autocorrelation curve (e.g., by lagging the

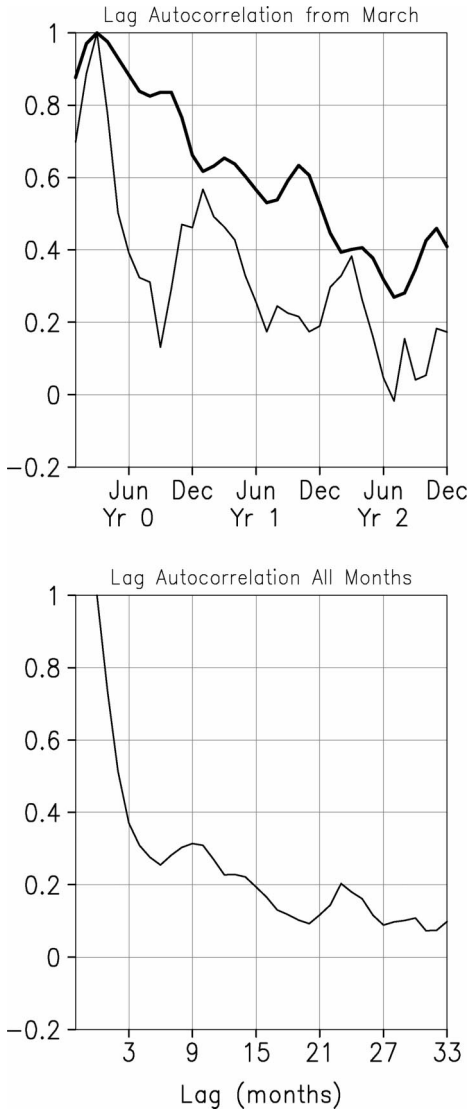

FIG. 3. (top) Monthly lag autocorrelation curves from Mar for the leading principal component time series of North Atlantic heat content anomalies (thick) and associated SST anomalies (thin). (bottom) Monthly lag autocorrelation curve for the SST record based upon all months.

monthly SST anomaly time series by 1 month, 2 months, . . . 36 months), the seasonal cycle virtually disappears, with a rapid decay to ~0.3 within first 3 months followed by a more gradual decline (Fig. 3, bottom). Thus, the SST *e*-folding timescale based upon all months of the year (~3 months) is considerably shorter than that obtained by considering only winter SST anomalies (~2–3 yr).

The leading EOF of monthly HC anomalies over the North Pacific is shown in Fig. 4 together with the climatological distribution of February mixed layer depths. The EOF, which accounts for 30% of the variance, exhibits a primary center of action along ~40°N that extends across the western two-thirds of the basin, and a

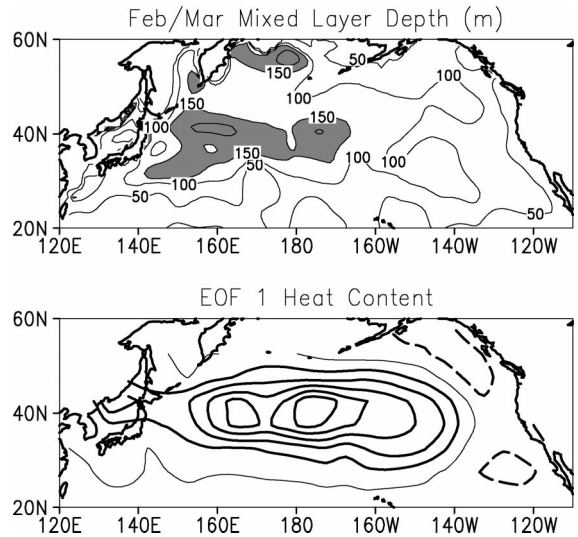

FIG. 4. As in Fig. 2 but for the North Pacific.

center of opposite polarity along the west coast of North America. As in the Atlantic, this pattern is similar to the leading EOF of monthly SST anomalies (not shown), but with a different spatial emphasis: more weight for the primary center of action where the winter mixed layers are deepest, and relatively less weight along the American coast where they are shallower. The lag autocorrelation curves for the HC PC and the associated SST projection time series starting from March are shown in Fig. 5. As in the Atlantic, the decay of the HC autocorrelations is nearly monotonic and resembles the attenuation rate for winter SST. Also as in the Atlantic, the summer (August–September) minima in the SST autocorrelation curve are absent from the HC curve, and the HC autocorrelations decay most rapidly in late fall and early winter, and least rapidly in late

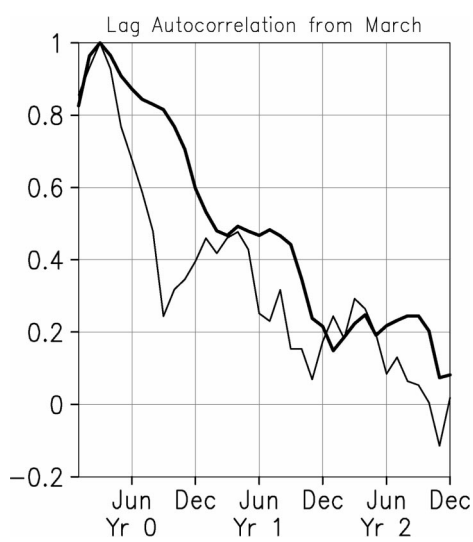

FIG. 5. As in Fig. 3 (top) but for the North Pacific.

spring and summer. The overall rate of decay of the HC autocorrelations is faster for the Pacific than the Atlantic, qualitatively consistent with the fact that the winter mixed layers depths are smaller in the Pacific than the Atlantic.

b. *An extension of the simple stochastic climate model: Implicitly incorporating the effect of entrainment*

To understand quantitatively the rate of attenuation of the lag autocorrelation curve of monthly HC anomalies (or equivalently, the rate of decay of winter SST autocorrelations), it is helpful to consider the formulation of FH77 in terms of H_{eff}. The governing equation for the simple stochastic climate model is

$$(\rho C_p H_{\mathrm{eff}}) dT'/dt = F' - \lambda T', \tag{1}$$

where ρ is the density of seawater (taken here as 1000 kg m^{-3}), C_p is the heat capacity of seawater (4128 J kg^{-1} K^{-1}), H_{eff} is the mean maximum mixed layer depth, T' is the mixed layer temperature anomaly, t is time, F' represents the atmospheric forcing of T', and λ is a linear damping coefficient. The linear damping term $\lambda T'$ is a highly idealized representation of the turbulent fluxes of latent and sensible heat flux from the ocean to the atmosphere associated with T'. Note that without damping, Eq. (1) would result in unbounded growth of T'.

The damping parameter λ may be derived by linearizing the bulk formulas for the sensible and latent energy fluxes about T', as shown in Haney (1985), Frankignoul (1985), Barsugli (1995), Barsugli and Battisti (1998), and Frankignoul et al. (1998). The magnitude of λ depends upon the strength of the near-surface wind speed and the degree to which the near-surface air temperature and relative humidity adjust to the underlying SST perturbation (see also Seager et al. 1995). For the North Atlantic and Pacific, λ is estimated to be in the range 15–20 W m^{-2} K^{-1}. These estimates may be compared with values obtained directly from atmospheric GCM experiments with an imposed SST anomaly and diagnosing the resulting change in the local surface turbulent energy flux. As reviewed by Frankignoul et al., these experiments yield annually averaged values ~10–20 W m^{-2} K^{-1} depending on location. A recent GCM study by G. Magnusdottir, C. Deser, and R. Saravanan (2002, unpublished manuscript) for a prescribed SST anomaly in the North Atlantic confirms this result, with λ ~15 W m^{-2} K^{-1}. Although difficult to obtain accurately from data, λ has been estimated on the basis of observed lagged covariances between turbulent heat flux and SST anomalies over the eastern North Atlantic by Frankignoul et al. (1998), with a range similar to that found in the atmospheric GCM experiments.

If F' in Eq. (1) is specified to be ''white'' in time, that is, the decorrelation timescale for atmospheric weather variations (on the order of a week) is much shorter than that for SST fluctuations (see FH77), then the autocorrelation function (r) of T' as a function of time lag τ is simply

$$r(\tau) = \exp\{-[\lambda/(\rho C_p H_{\mathrm{eff}})]\tau\} \tag{2}$$

According to (2) with constant λ, T' decays exponentially at a rate proportional to the inverse of H_{eff}: the deeper the mixed layer, the slower the rate of attenuation due to the larger thermal inertia. In the following analysis, we shall compare the theoretical autocorrelation function given by (2) with observed autocorrelation curves for HC and winter SST for selected regions, using observed long-term mean values for H_{eff} from Monterey and Levitus (1997). We shall refer to Eq. (2) as the extended simple stochastic climate model.

c. *Regional analyses and application of the extended simple stochastic climate model*

We have selected two regions for analysis, each the dominant center of action of the leading EOF of monthly HC anomalies in their respective basins: the northern North Atlantic (45°–60°N, 45°–20°W; hereafter referred to as NATL) and the western central North Pacific (35°–45°N, 155°E–170°W; hereafter referred to as NPAC). Monthly lag autocorrelation curves based upon March SST and HC anomaly time series for NATL and NPAC are shown in Figs. 6a and 6b, respectively [results based upon linearly detrended data are similar, with a small (~0.05–0.10) reduction in the autocorrelation values, which is approximately uniform with lag; not shown.] Also shown are the theoretical autocorrelation curves from Eq. (2) with H_{eff} given by the observed February climatological mixed layer depth (367 m for NATL and 178 m for NPAC) and λ in the range 15–20 W m^{-2} K^{-1}. The observed HC and SST autocorrelation curves exhibit many of the same features as found in the EOF-based results: a nearly monotonic decay for HC and a pronounced seasonal cycle for SST, with minima in summer and maxima in winter. The winter SST autocorrelation magnitudes are similar to the concurrent HC values. The theoretical decay based upon H_{eff} (shaded region in Fig. 6) exhibits good agreement with the observed decay of HC and winter SST autocorrelations in both regions. Given the simplicity of the model and the lack of ''tuning'' of parameters (λ, H_{eff}), the fit between observations and theory is highly encouraging. One notable difference between the two regions is the stronger seasonal variation in the SST autocorrelation curve, due principally to the lower values in summer, in NPAC than in NATL.

The SST autocorrelation curves exhibit a rapid decline within the first 6 months, reaching a minimum in September in both regions. What controls the rate of attenuation of SST anomalies from March to September? The original formulation of FH77 is applicable here, given that entrainment is weak during this half of the year when the mixed layer is either shoaling (in spring) or steady (in summer). Accordingly, we have

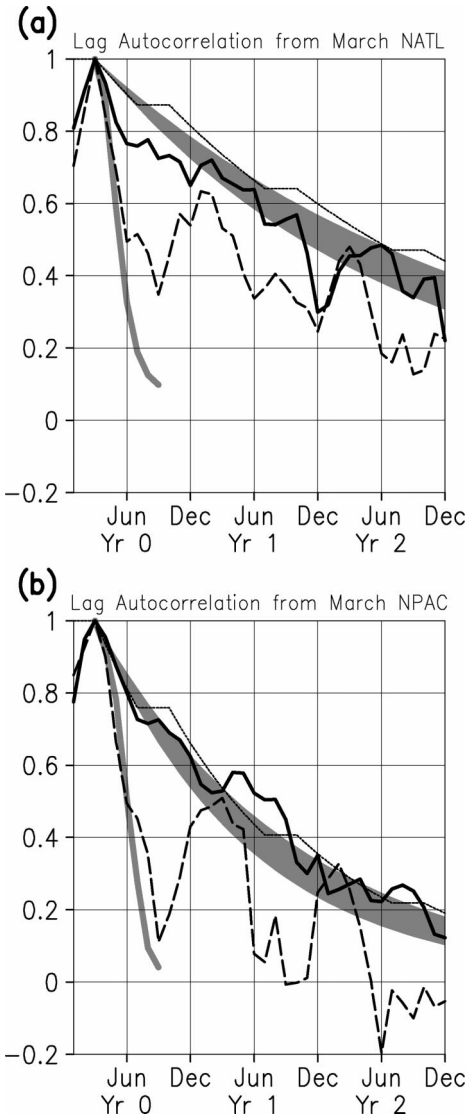

FIG. 6. Observed monthly lag autocorrelation curves from Mar for heat content (thick black) and SST (dashed) anomalies in the (a) NATL and (b) NPAC regions. The broad band of shading denotes the theoretical autocorrelation function from the extended simple stochastic climate model. The thin gray curve that ends in Sep of year 0 denotes the theoretical autocorrelation function from the original model. The thin black curve denotes the theoretical autocorrelation function from the extended simple stochastic climate model with zero damping in summer (see text for details).

calculated the theoretical autocorrelation curve from Eq. (2) using observed long-term mean monthly values of mixed layer depth from March through September for each region and $\lambda = 17.5$ W m^{-2} K^{-1} based on a simple forward time stepping technique. The resulting theoretical autocorrelation function (gray curve in Fig. 6b) approximates well the observed SST autocorrelation curve in the NPAC region. Thus, winter SST anomalies in the NPAC region decay through summer at a rate consistent with the simple (nonentraining) stochastic climate model. In the NATL region, the theory fits the initial rate of decay of the observed SST autocorrelation curve within the first 2–3 months, but then strongly underestimates the values from July to September.

In Eq. (1), we have treated the mixed layer as a fixed-depth slab ($H = H_{\mathrm{eff}}$) whose temperature anomaly T' damps to the atmosphere at a constant rate λ. However, in summer, the fossil winter mixed layer becomes effectively isolated from the atmosphere due to the formation of a warm thin surface layer and thus temperature anomalies within this layer do not damp to the atmosphere. Therefore, the damping parameter for HC$'$ should be nearly zero in the summer months, unlike that for SST$'$. To illustrate the impact of a seasonally varying damping rate, we use a simple binary specification of λ in Eq. (2): zero in the summer months (July–September) and 20 W m^{-2} K^{-1} in the remaining months (note that λ in this context should be interpreted as the effective damping rate for HC$'$ and not for SST anomalies per se). As expected, the theoretical autocorrelation function with zero damping in summer (thin solid curve in Figs. 6a,b) decays less rapidly than that with constant year-round damping, but the differences are relatively small ($\sim$0.1). Given the empirical nature of λ to begin with, we do not consider it useful at this stage to pursue a more complicated formulation for the seasonal dependence of λ.

d. Atmospheric forcing

Our analyses and interpretation of the results within the framework of the simple stochastic climate model are predicated on the assumptions that 1) the atmosphere is forcing the winter SST anomalies, and 2) the atmospheric forcing has a short decorrelation timescale (a week or two) with a white-noise power spectrum at lower frequencies (see FH77). In this section, we investigate to what extent these assumptions are valid for the NATL and NPAC regions. Previous studies indicate that the primary forcing terms in winter are the turbulent fluxes of sensible and latent heat, and horizontal temperature advection by Ekman currents (cf. Cayan 1992; Frankignoul and Reynolds 1983; Deser and Timlin 1997; Frankignoul et al. 1998; Seager et al. 2000, 2001). Note that Ekman currents are set up nearly instantaneously in the ocean mixed layer as a response to the local wind stress, and produce SST variations by advecting the background SST gradient. We shall refer to the sum of the fluxes of sensible and latent heat and Ekman advection as F'. Figure 7 (top) shows the monthly lag cross correlations between F' and the anomalous SST in March (the base month used for the SST autocorrelation curves shown previously) for both NATL and NPAC. The cross correlations are shown for F' from the previous October through the following September relative to the SST anomaly in March. Positive (negative) values denote the atmosphere is forcing (damping) SST. A correlation coefficient exceeding 0.21 in absolute value is significantly different from zero at the 5%

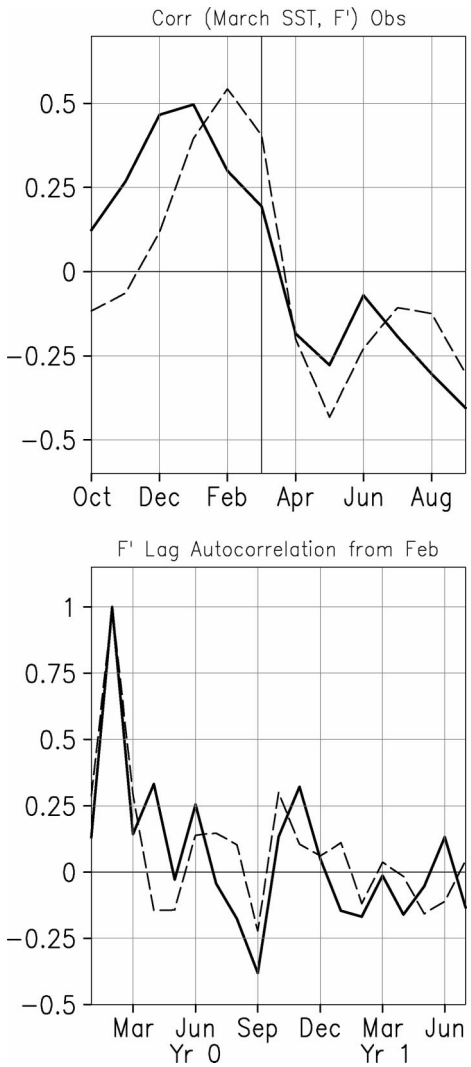

FIG. 7. (top) Lag cross correlations between Mar SST and monthly atmospheric forcing (F') from the previous Oct through the following Sep for NPAC (solid) and NATL (dashed). (bottom) Monthly lag autocorrelations for F' starting from Feb for NPAC (solid) and NATL (dashed).

confidence level. The results show that the strongest positive correlations (~0.5) occur when the atmosphere leads SST by 1–2 months, consistent with our assumption of atmosphere forcing and with the results of numerous previous studies (cf. Davis 1976; Cayan 1992; Deser and Timlin 1997; FH77). The magnitude of the maximum cross correlation is in excellent quantitative agreement with simple stochastic climate model theory (see appendix in FH77). Negative correlations, indicative of SST anomalies dampling to the atmosphere, occur when SST lags the atmosphere by 1–6 months, also consistent with previous studies (e.g., Frankignoul et al. 1998; Kushnir et al. 2002).

Does F' exhibit any substantial winter-to-winter autocorrelation that might contribute to the observed winter-to-winter persistence in SST, thereby diminishing the role for the reemergence mechanism? Figure 7 (bottom) shows the lag autocorrelation curves for F' starting from February (other winter months give similar results). The value F' exhibits a rapid decorrelation timescale (~1 month), with weak (generally less than 0.2 in absolute value) autocorrelations at longer lags, consistent with more comprehensive analyses of atmospheric decorrelation timescales (cf. FH77; Alexander and Penland 1996). The autocorrelation of F' from one winter to the next is also small (~0.1–0.2). Whether this small positive winter-to-winter autocorrelation has any appreciable influence upon winter SST anomaly persistence remains to be seen.

4. Further modeling results

Next we employ two additional models to investigate the role of entrainment in accounting for the seasonal dependence of winter SST anomaly persistence. The first is an explicit treatment of entrainment within the framework of the simple stochastic climate model of FH77; the second is an atmospheric general circulation model coupled to a ''full-physics'' entraining ocean mixed layer model.

a. The explicit ''entraining'' simple stochastic climate model

Here we propose an extension of the simple stochastic climate model that explicitly incorporates entrainment and hence allows for the reemergence mechanism; we shall refer to this system as the entraining stochastic climate model. We modify Eq. (1) to include a variable-depth mixed layer $H(t)$ that undergoes an identical seasonal cycle each year and an entrainment velocity $W_e = dH/dt$ if the mixed layer is deepening and zero if the mixed layer is steady or shoaling. With the addition of this term, the entraining simple stochastic climate model may be written as

$$(\rho C_p)d(HT)'/dt = F' - \lambda T' + (\rho C_p W_e)(T' - T'_b), \quad (3)$$

where T'_b is the temperature anomaly below the mixed layer, formed at an earlier time t_e. Note that t_e is a function of the seasonal cycle of mixed layer depth: that is, a temperature anomaly existing at a depth k in a particular year will persist beneath the summer mixed layer at that depth and be recaptured into the mixed layer during the following winter when it deepens again to depth k. Equation (3) was numerically solved for $T'(z)$ using a time step of 3 days, a vertical resolution of 40 levels between the surface and the maximum mixed layer depth, and integrated for 5000 yr. For the integrations, a maximum and minimum value for $H(t)$ is prescribed, with the added specification that the mixed layer shoals for 4 months, remains steady for 4 months, and deepens for 4 months. The damping parameter λ is prescribed to vary sinusoidally over the annual cycle, with a maximum value of 25 W m^{-2} K^{-1} in February

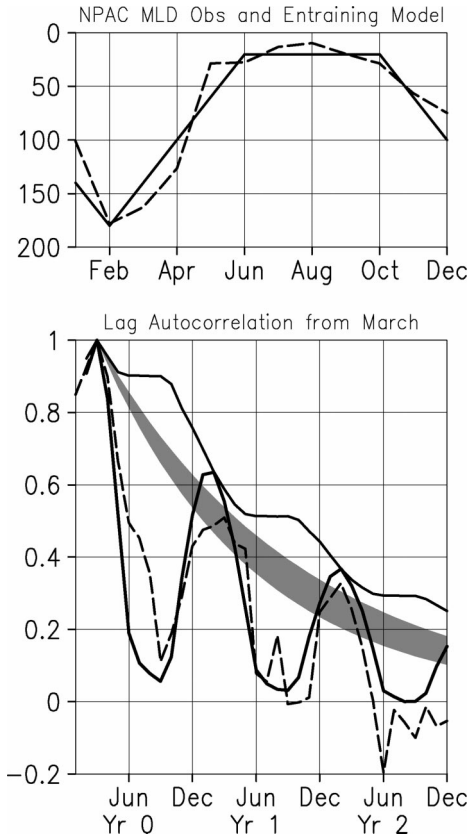

FIG. 8. (top) Mean seasonal cycle of mixed layer depth (m) for NPAC from observations (dashed) and that used in the entraining stochastic climate model (solid). (bottom) Monthly lag autocorrelation curves from Mar for heat content (solid step functionlike curve) and SST (solid) from the entraining model. The observed SST autocorrelation curve is dashed. The theoretical autocorrelation function for heat content based upon the extended simple stochastic climate model is shaded.

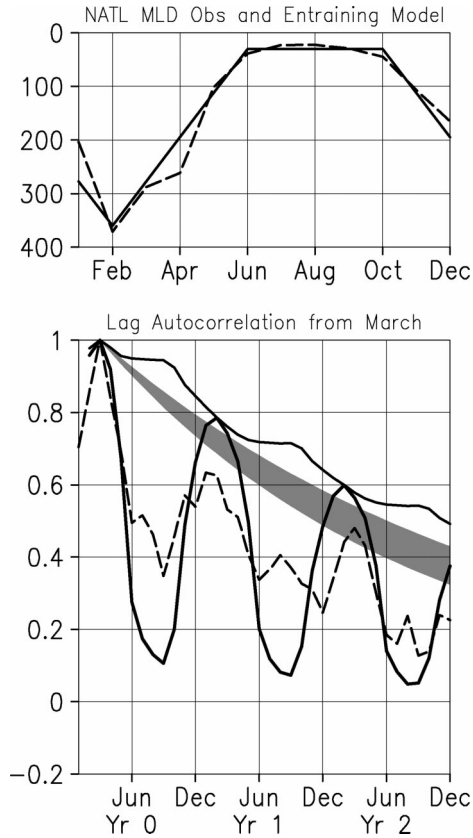

FIG. 9. As in Fig. 8 but for the NATL region.

and a minimum value of 5 W m^{-2} K^{-1} in August according to the atmospheric GCM results of G. Magnusdottir, C. Deser, and R. Saravanan (2002, unpublished manuscript). We note that the location of the imposed SST anomaly in their experiments corresponds closely to our NATL region. We note further that the atmospheric GCM experiments of Peng et al. (1997) for an imposed SST anomaly in the North Pacific that corresponds closely to our NPAC region yields wintertime values for λ of 25–30 W m^{-2} K^{-1} (other months were not examined in their study).

Figure 8 (top) shows the seasonal cycle of the observed long-term monthly mean mixed layer depth for NPAC and the one we specify for the model integration. The idealized seasonal cycle approximates the observed seasonal evolution of mixed layer depth. The resulting lag autocorrelation curves for SST and HC from the simple model, and the observed SST, based upon a starting month of March are shown in the bottom portion of Fig. 8. The entraining model agrees well with the observations in terms of the timing and magnitudes of the summer minima and winter maxima. The main shortcomings of the model are the underestimation of the autocorrelations in June–August of the first year and slight overestimation of the winter values. Given the simplicity of the model, the agreement is encouraging. To benchmark this model against the extended or ''implicit-entraining'' stochastic climate model [Eq. (2)], the exponentially decaying autocorrelation curves based upon H_{eff} and λ in the range 15–20 W m^{-2} K^{-1} are also shown in Fig. 8. The implicit-entraining model provides a good approximation to the ''explicit-entraining'' model in terms of the winter-to-winter autocorrelations in SST and HC. Figure 9 shows the results for the NATL region. Although the timing of the summer minima and winter maxima in the observed SST autocorrelations is well simulated, the model overestimates the values in winter and strongly underestimates the values in the first and second summers.

b. A full-physics ocean mixed layer model coupled to an atmospheric GCM

The most complex ocean–atmosphere configuration in our model hierarchy is a full-physics ocean mixed layer model coupled to an atmospheric GCM. Compared to the simple stochastic climate models, this configuration is a more realistic representation of the relevant

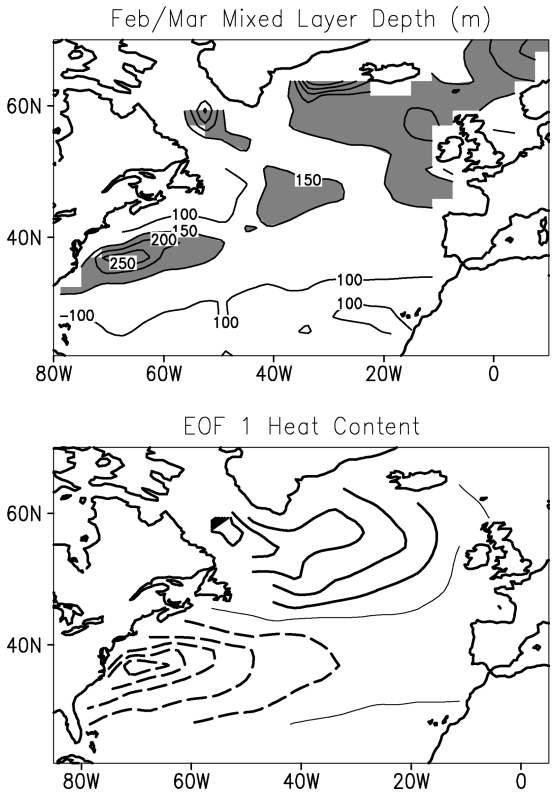

FIG. 10. As in Fig. 2 but for the 16-member ensemble of coupled ocean mixed layer–atmospheric GCM integrations.

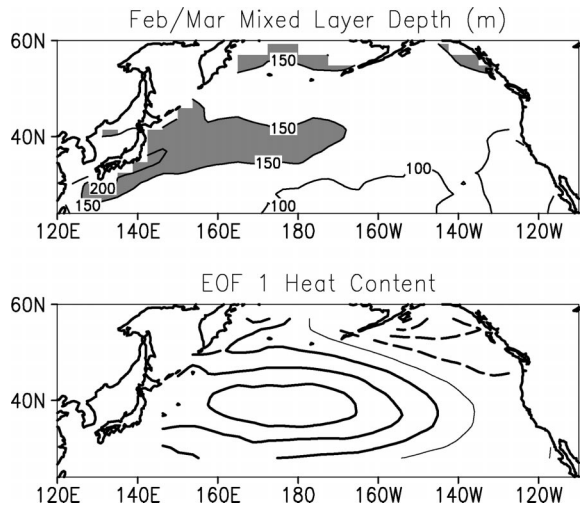

FIG. 11. As in Fig. 10 but for the North Pacific.

physical processes of atmosphere–ocean mixed layer interaction including the reemergence mechanism. For example, atmospheric forcing of the ocean mixed layer is no longer assumed to be white noise, the rate of damping of SST anomalies back to the atmosphere is not assumed to be constant, and the entrainment rate in the ocean model is derived from the turbulent kinetic energy equation. We make use of an ensemble of 16 integrations of this coupled model as described in Alexander et al. (2002). Each integration spans the period 1950–99 and consists of prescribed monthly SST anomalies in the eastern tropical Pacific (15°N–15°S, 172°E–South American coast) taken from observations and the ocean mixed layer model elsewhere. This configuration is designed to incorporate boundary forcing due to variability associated with the El Niño–Southern Oscillation (ENSO) phenomenon whose governing dynamics are not described by mixed layer processes. The ocean model consists of a grid of one-dimensional bulk mixed layer models atop a simple layered model representative of the thermocline; each ocean column is coupled to the atmospheric column above it, but there is no communication between adjacent grid cells in the ocean model. The bulk mixed layer model, based on Gaspar (1988), contains a prognostic formulation for mixed layer depth and entrainment. Beneath the mixed layer, heat is redistributed via convective overturning, vertical diffusion, and penetrating solar radiation. The atmospheric model is the Geophysical Fluid Dynamics Laboratory (GFDL) R30 GCM which has an equivalent horizontal resolution of ~2.25° in latitude and 3.75° in longitude and 14 sigma levels in the vertical.

The model output was analyzed in the same manner as the observations, including EOF analysis of monthly SST and HC anomalies in the North Atlantic and Pacific basins, and regional analyses based upon the main centers of action of the leading EOF in each basin. For all analyses, the 16 integrations were appended to form one long record to provide a more robust representation of the model's variability.

Figure 10 shows the leading EOF of monthly heat content anomalies in the North Atlantic together with the long-term mean February MLD. The distribution of MLD in the model is similar to observations (recall Fig. 2), with higher values in the northern portion of the basin extending in a narrow tongue toward the southwest. However, the model strongly underestimates the MLD in the north (maximum values ~200–300 m compared to 300–800 m in observations). The leading EOF, which accounts for 34% of the variance, exhibits a north–south dipole pattern, similar to observations. Unlike observations, the two centers of action are comparable in strength, in line with their similar February MLDs.

The leading EOF of monthly heat content anomalies in the North Pacific together with the long-term mean February MLD is shown in Fig. 11. The model simulates well the distribution of MLD, with higher values along ~40°N in the western portion of the basin and in the Bering Sea. The leading EOF, which accounts for 35% of the variance, closely resembles observations, with a primary center of action along 40°N extending across the western two-thirds of the basin and a second center of opposite polarity in the Gulf of Alaska. Unlike ob-

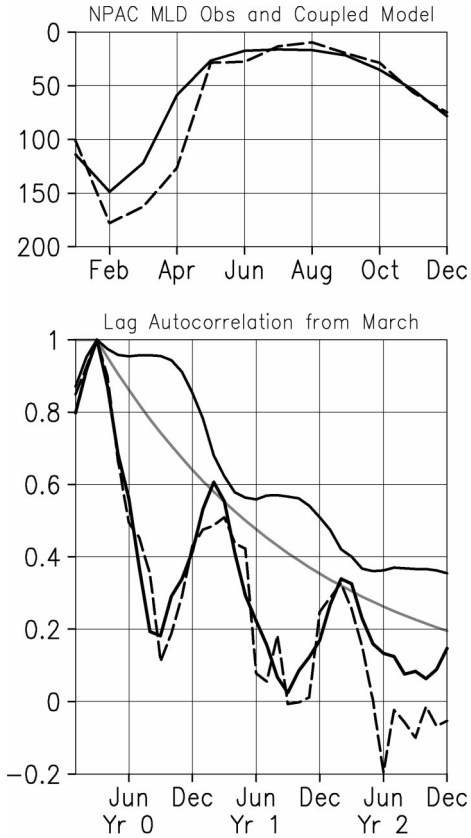

FIG. 12. (top) Mean seasonal cycle of mixed layer depth (m) in the NPAC region from observations (dashed) and the coupled model (solid). (bottom) Monthly lag autocorrelation curves from Mar for heat content (solid steplike curve) and SST (solid) from the coupled model. The observed SST autocorrelation curve is dashed. The theoretical autocorrelation function for heat content based upon the extended simple stochastic climate model is the thin gray exponential curve.

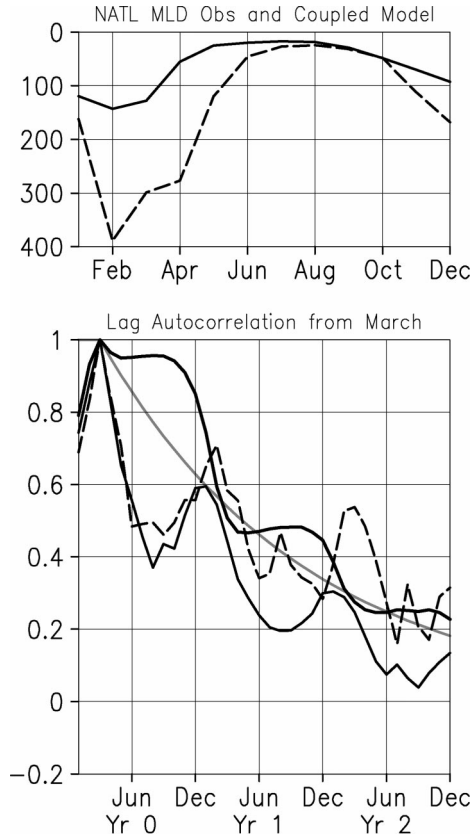

FIG. 13. As in Fig. 12 but for the coupled model's NATL region.

servations, the two centers are of comparable strength, in line with their similar February MLDs.

Figure 12 (top) shows the seasonal cycle of the observed long-term monthly mean mixed layer depth for model's equivalent of the NPAC region defined as the center of action of the leading EOF in the Pacific (33°–46°N, 154°–191°E). The model approximates well the observed seasonal evolution of mixed layer depth, although it is somewhat too shallow at the time of maximum extent in February (143 m compared to 178 m in observations) and shoals most rapidly from March to April, about 1 month ahead of nature. Figure 12 (bottom) shows the monthly lag autocorrelations of the model's NPAC SST and HC anomalies starting from March; the observed SST autocorrelations are also shown for comparison. The model's HC autocorrelation curve exhibits a rapid decay during the months of mixed layer deepening (November–February), consistent with the effect of entrainment, which mixes or dilutes the existing heat content anomaly with thermal anomalies newly formed by wintertime atmospheric forcing, and little attenuation during the months when the mixed layer shoals or remains steady (April–October). The SST autocorrelation curve from the model is very similar to observations, including the magnitude and timing of the summer minima and winter maxima. The theoretical autocorrelation curve based on the extended simple stochastic climate model [Eq. (2)] with H_{eff} given by the model's long-term mean February mixed layer depth and $\lambda = 12\ \mathrm{W\ m^{-2}\ K^{-1}}$ provides an excellent fit to the model's SST correlations from winter to winter [note that the annually averaged damping parameter that fits the model the best is somewhat smaller than the range of values used to benchmark the observations against (15–20 $\mathrm{W\ m^{-2}\ K^{-1}}$), possibly because vertical diffusion through the main thermocline also acts to damp mixed layer temperature anomalies in the model].

The results for the model's equivalent of the NATL region, given by the center of action of the leading EOF in the Atlantic (52°–59°N, 49°–26°W), are shown in Fig. 13. The seasonal cycle of mixed layer depth is not well simulated due to the lack of deep winter mixing (the model's maximum value is 149 m in February, compared to an observed value of 390 m). Consistent with the shallower winter mixed layer, the model exhibits a stronger attenuation of the SST autocorrelation curve compared to observations. As for NPAC, the theoretical autocorrelation curve based on the extended simple sto-

chastic climate model with $\lambda = 12$ W m^{-2} K^{-1} provides an excellent fit to the model's SST correlations from winter to winter.

Like observations, the model produces a substantial difference in the level of the winter-to-summer SST autocorrelations between the NATL and NPAC regions. In NPAC, the summer SST anomalies are practically uncorrelated ($r \sim 0.2$) with those in the previous winter in both the model and observations, while in NATL they are substantially correlated ($r \sim 0.4$–0.5) in both model and nature. The fact that the model, with 16×50 yr of record, reproduces this aspect of the observations (with only 50 yr of record), suggests that this is a real feature of both the model and nature. One possible reason for the different behavior in the Atlantic and Pacific is that the static stability within the seasonal thermocline beneath the summer mixed layer is weaker in NATL than in NPAC (not shown) such that episodic entrainment events during summer are more effective in bringing temperature anomalies stored within the seasonal thermocline up into the mixed layer, resulting in higher SST anomaly persistence from winter to summer.

One of the benefits of the coupled ocean mixed layer–atmospheric GCM configuration is that the atmospheric forcing of SST anomalies is not assumed to be a white noise process as was the case for the implicit- and explicit-entraining stochastic climate models. In view of this, and given the potential influence of ENSO teleconnections on the characteristics of atmospheric variability over the North Pacific and Atlantic (see Alexander et al. 2002), we examine the model's atmospheric forcing over the NPAC and NATL regions. Note that the primary atmospheric forcing of SST anomalies in the model is the net surface heat flux, which includes the turbulent fluxes of latent and sensible heat, and shortwave and longwave radiation: there are no Ekman currents. Figure 14 (top) shows the lag cross correlations between the time series of SST anomalies in March (the base month used for the SST autocorrelation curves shown above) and the time series of the net surface heat flux (Q) from the previous October through the following March for NPAC and NATL. The strongest positive correlations ($\sim$0.4 and 0.5 for NPAC and NATL, respectively) are found when the atmosphere leads SST by 1–2 months, and negative correlations occur when SST lags the atmosphere by 1–6 months, similar to observations in both timing and magnitude (recall Fig. 7). The monthly lag autocorrelations of Q' starting from February (Fig. 14, bottom) show that the model's atmospheric forcing decorrelates within $\sim$1 month and exhibits no winter-to-winter autocorrelation, again similar to observations.

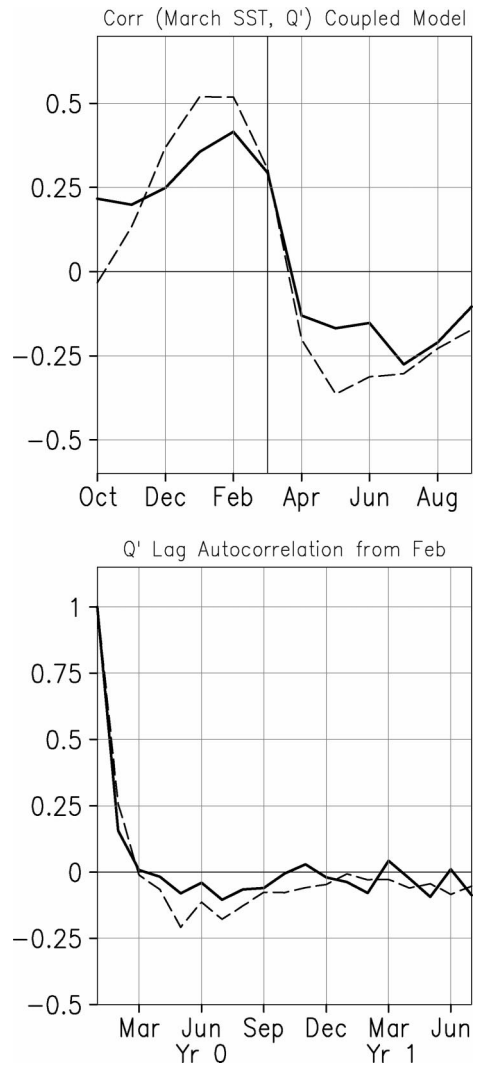

FIG. 14. As in Fig. 7 but for the coupled model.

5. Additional results

a. Basinwide patterns of winter-to-winter SST autocorrelations

Here we examine more generally the relevance of the extended simple stochastic climate model by comparing the spatial patterns of winter-to-winter SST autocorrelations at each grid point over the northern oceans from observations and theory. The observed autocorrelations are computed between the time series of SST anomalies in March and those in February of the following year (this choice is motivated by the monthly lag autocorrelation curves for NATL and NPAC, see Fig. 6). The theoretical autocorrelations are computed from Eq. (2) with H_{eff} given by the long-term mean February/March MLDs from observations and $\lambda = 20$ W m^{-2} K^{-1}.

In the observations (Fig. 15a), the highest winter-to-winter autocorrelations occur in the northern North Atlantic, with values in the range 0.5–0.75. A tongue of relatively high correlations (0.3–0.5) extends from the northern North Atlantic southwestward toward the eastern seaboard of the United States. Relatively high correlations also occur along the coastal margins of West Africa and between Cape Hatteras and Nova Scotia. In the Pacific, a band of high autocorrelations (0.3–0.5) is

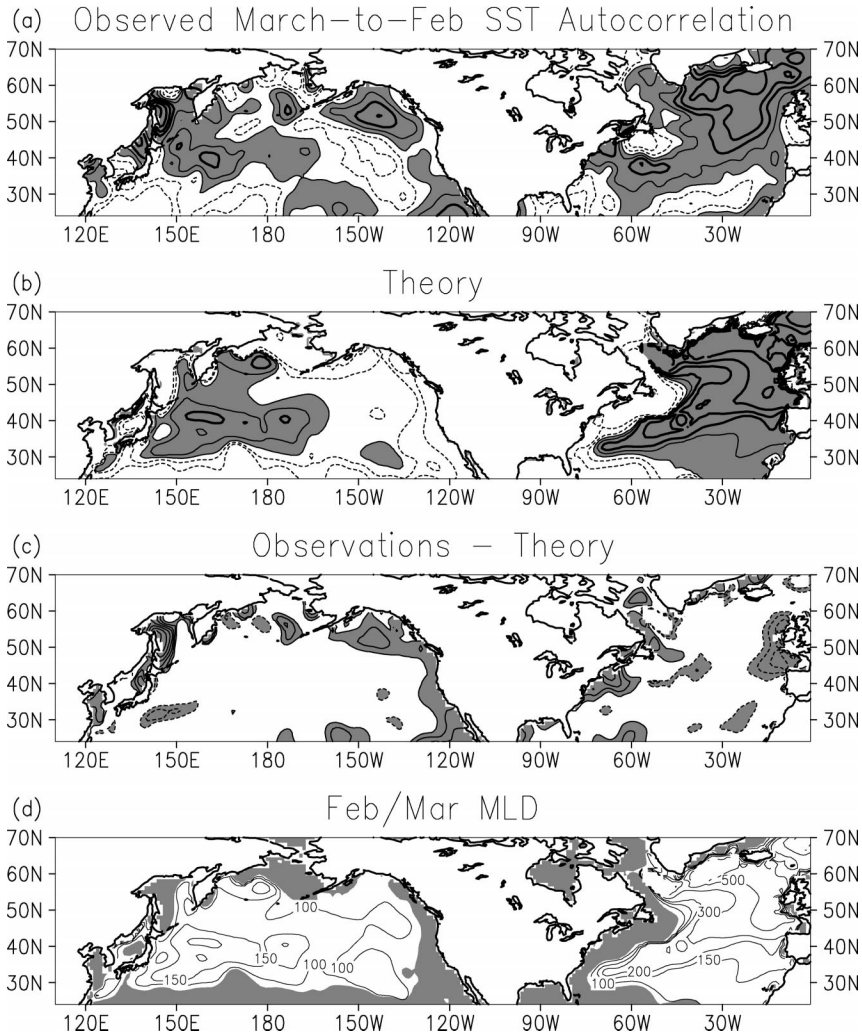

FIG. 15. Local SST anomaly autocorrelations from Mar to the following Feb based upon (a) observations and (b) the extended simple stochastic climate model. The contour levels are 0.1 and 0.2 (dashed), 0.3 and 0.4 (thin solid) and 0.5, 0.6 and 0.7, and 0.8 (thick solid); values $>$ 0.3 are shaded. Note that there are no values $<$ 0. (c) Observed minus theoretical autocorrelations [(a) minus (b)]. The contour interval is 0.1, starting at ± 0.2. Positive (negative) contours are solid (dashed), and values $>$ 0.2 and <-0.2 are shaded. (d) Observed long-term mean winter mixed layer depths. The contour levels are 100, 150, 200, 300, 500, and 800 m. Shading denotes locations where the mean annual cycle in mixed layer depth (Feb/Mar minus Aug) is less than 60 m.

found along ~40°N in the western half of the basin, in the Gulf of Alaska, the southeastern Bering Sea, and west of Baja California. High correlations are also found in the Sea of Okhotsk, the Sea of Japan and off Kamchatka. Elsewhere, the correlations are ~0.1–0.2.

The broad features of the observed autocorrelation distribution are evident in the simple theoretical results (Fig. 15b). In particular, the highest values are found in the northern North Atlantic (0.5–0.8), with a tongue of relatively high values (0.3–0.6) extending southwestward across the Atlantic, and a band of high values (0.3–0.5) along ~40°N in the western Pacific extending northward along the western margin; elsewhere the correlations are ~0.1–0.2. The main deficiencies in the model are the lack of high autocorrelations in the Gulf of Alaska, off Baja California, the Sea of Okhotsk, the Sea of Japan, and between Cape Hatteras and Nova Scotia. These discrepancies between the observed and theoretical values are highlighted in the difference map (Fig. 15c). This map also indicates that the model overestimates the autocorrelations directly west of France and Great Britain, and in a small region directly southeast of Japan.

The theory tends to underestimate the observed autocorrelation values in coastal regions where the seasonal variation in mixed layer depth is small (see Fig.

15d). Although the impact of reemergence upon winter SST anomaly persistence should be weak in these areas, other processes such as those associated with ocean dynamics may play a role. For example, previous studies have suggested that anomalous geostrophic thermal advection may be important for winter SST variability between Cape Hatteras and Nova Scotia (Bhatt et al. 1998; Seager et al. 2000) and in the Gulf of Alaska (Lagerloef 1995). Similarly, anomalous thermal advection by coastal Kelvin waves and reflected Rossby waves that occur in association with ENSO (Miller et al. 1997) may contribute to SST variability west of Baja California. The high autocorrelation values in the Sea of Japan and Sea of Okhotsk may be related to sea ice variability.

Uncertainties in the observational estimates of H_{eff} may also contribute to discrepancies between the observed and theoretical autocorrelation values. There are several sources of error in H_{eff}, including paucity of data and inadequate sampling of its temporal variability (within a month and between years), and sensitivity to the criterion used to define mixed layer depth. While it is difficult to give a quantitative assessment of these errors, we note that other datasets yield broadly similar distributions of H_{eff}. We also note that a given percentage error in H_{eff} yields a smaller corresponding percentage error in the 1-yr lag autocorrelation of winter SST′ computed from Eq. (2) for $H_{\mathrm{eff}} > \sim 130$ m.

Given the simplicity of the model (e.g., use of a constant damping parameter and climatological values for H_{eff}), the overall agreement between theory and nature is encouraging (the pattern correlation between the observed and predicted autocorrelation distributions is 0.61). Recall that without the use of H_{eff} in the simple stochastic climate model (that is, without the implicit effects of entrainment and the reemergence process), the winter-to-winter lag autocorrelations would be zero everywhere. The rms difference between the observed and theoretical autocorrelation distributions (excluding grid points where the mean seasonal variation in mixed layer depth is <60 m) is 0.15, compared to 0.34 when the observations are benchmarked against the original FH77 theory. For the Pacific (Atlantic) basin alone, the rms difference is 0.13 (0.17) compared to 0.31 (0.39) with the original theory. A comparison between the winter SST autocorrelation distributions from the 16 coupled ocean mixed layer–atmospheric GCM integrations and theory (not shown) indicate a similar level of agreement (0.65 pattern correlation) as between observations and theory. Spatial variations in λ and interannual variations in H_{eff} presumably account for much of the remaining unexplained covariance.

6. Discussion

The simple stochastic climate model of FH77 has been widely adopted as the leading paradigm for the null hypothesis of SST variability in middle and high latitudes, whereby the ocean mixed layer integrates white noise atmospheric forcing to produce a red noise SST response. In this view, the predictability or persistence of SST anomalies is limited to the timescale associated with the thermal inertia of the mixed layer, a timescale determined by the depth of the mixed layer and the rate at which the SST anomaly damps to the atmosphere via turbulent heat fluxes. This paradigm has been used as a benchmark of comparison for diagnosing the contribution of other processes upon SST variability such as wind- and buoyancy-driven ocean currents and two-way ocean–atmosphere coupling (cf. Manabe and Stouffer 1988; Blade 1997; Seager et al. 2000, 2001; Pierce et al. 2001). The results of this study suggest that a more relevant null hypothesis for interannual SST variability in middle latitudes is the entraining stochastic climate model, or more simply, a reformulation of FH77 in terms of an effective mixed layer depth given by the maximum wintertime value. Adopting this paradigm augments the winter-to-winter persistence of SST anomalies considerably above the original model, which yields virtually no memory from winter-to-winter due to the ''resetting'' of thermal conditions each summer when the mixed layer shallows and the associated heat storage is minimal. Figure 16 illustrates the 1-yr lag autocorrelations and *e*-folding timescales for winter SST anomalies from the extended stochastic climate model as a function of H_{eff} and λ in the range 15–20 W m^{-2} K^{-1} (shading). Winter mixed layer depths typical of the North Pacific (100–200 m) are associated with 1-yr lag autocorrelations in the range 0.25–0.58 and *e*-folding timescales in the range 0.8–1.8 yr. The deeper winter mixed layers of the northern North Atlantic (300–550 m) are characterized by autocorrelations and *e*-folding times in the range 0.6–0.8 and 2–5 yr, respectively. Note that the use of a 50-m fixed-depth slab mixed layer common to many studies (e.g., Manabe and Stouffer 1988; Blade 1997; Pierce et al. 2001) yields a 1-yr autocorrelation of only 0.1 and an *e*-folding timescale of only 5 months, values that could lead to misinterpretation of the potential influence of the thermal inertia associated with the ocean mixed layer upon atmospheric variability.

The higher persistence of winter SST anomalies in the entraining or extended stochastic climate model means that it is more difficult to discern the influence of other processes such as internal ocean dynamics against the red noise background of SST variability due solely to stochastic atmospheric forcing. For example, SST fluctuations in the far North Atlantic where winter mixed layers are ~500-m deep may be expected to persist for ~5 yr even though they are being forced by random (e.g., unpredictable beyond a week or two) atmospheric fluctuations. Note that the reemergence mechanism does not lead to enhanced variance of winter SST anomalies in the interannual band as might be expected intuitively: rather, it acts as a reddening process, enhancing the variability at low frequencies compared

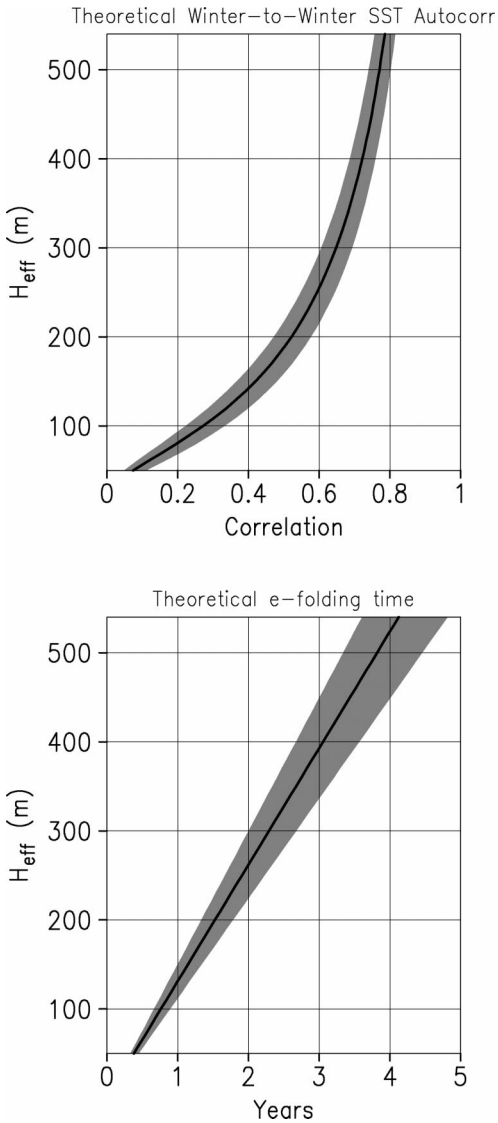

FIG. 16. Theoretical (top) 1-yr lag winter SST autocorrelations and (bottom) *e*-folding timescales as a function of winter mixed layer depth (H_{eff}) based upon the extended simple stochastic climate model.

to high frequencies. The reddening effect of the reemergence process can be understood in light of the simple heuristic model presented in Eq. (2). The deeper the effective mixed layer depth, the greater the associated thermal inertia and integrating effect of the ocean mixed layer of short timescale weather variations, and hence the longer the persistence of winter SST anomalies.

Although the simple extension we propose to the model of FH77 yields encouraging results, several of the simplifying assumptions we have made should be scrutinized in future work. One such assumption is the use of a long-term mean winter mixed layer depth for H_{eff} rather than one that varies year by year. Anomalies in H_{eff} may impact the strength of the reemergence mechanism in at least two ways: first, H_{eff} may be correlated with the amplitude of the concurrent winter SST anomaly (the deeper the mixed layer, the smaller the temperature anomaly for the same atmospheric forcing), and second, winter mixed layer temperature anomalies may impact the stratification the following winter, which would affect H_{eff} and hence temperature anomalies. It will be worth examining these effects when reliable gridded datasets of monthly mixed layer depth become available for a sufficiently long period of record. The modeling results of Alexander et al. (2000) suggest, however, that these effects are of secondary importance compared to the impact of the mean seasonal cycle of mixed layer depth.

Another obvious simplification in the model is the use of a constant damping parameter λ. While we have purposely chosen not to tune this parameter in the present study, it would be useful to examine the sensitivity of the results to a more realistic distribution of λ in both space and time. Unfortunately, at the present time, spatial and seasonal variations of λ are difficult to estimate with sufficient accuracy from the available observations (see Frankignoul et al. 1998). In the 16-member ensemble of coupled integrations, λ is free to vary in both time and space. Investigation of the impact of a variable damping rate upon SST persistence in the coupled model configuration will be the subject of future work.

The results of this study do not preclude the potential importance of oceanic processes such as advection, diffusion, eddy mixing, and subduction upon the persistence of mixed layer temperature anomalies. The recent studies of Qiu (2002) and Schneider and Miller (2001; see also Seager et al. 2001) indicate that both the reemergence mechanism and geostrophic advection influence the upper-ocean heat balance and generation of winter SST anomalies along the Kuroshio Current Extension, with the former dominating SST anomaly persistence at 1–2-yr timescales and the latter becoming more important at longer timescales. De Coetlogon and Frankignoul (2003) estimate that *e*-folding timescales for winter SST anomalies along the Gulf Stream and in the subpolar North Atlantic increase by 3–7 months when mean advection is taken into account. Further quantitative assessment of the effects of dynamical ocean processes versus mixed layer physics (e.g., the reemergence mechanism) is needed for a more complete understanding of interannual and longer timescale SST variability in midlatitudes.

Acknowledgments. We thank Dr. R. Saravanan for useful discussions and for help with coding the entraining stochastic climate model. We also thank Adam Phillips and Jamie Scott for their technical assistance. Helpful comments and suggestions were provided by an anonymous reviewer and Drs. T. Joyce, B. Qiu, F. Straneo, and M. Visbeck. This work was supported in part by grants from NOAA's OGP CLIVAR Program. The

figures were produced with GrADs software courtesy of the University of Maryland.

REFERENCES

Alexander, M. A., and C. Deser, 1995: A mechanism for the recurrence of wintertime midlatitude SST anomalies. *J. Phys. Oceanogr.,* **25,** 122–137.

——, and C. Penland, 1996: Variability in a mixed layer model of the upper ocean driven by stochastic atmospheric surface fluxes. *J. Climate,* **9,** 2424–2442.

——, C. Deser, and M. S. Timlin, 1999: The reemergence of SST anomalies in the North Pacific Ocean. *J. Climate,* **12,** 2419–2433.

——, J. D. Scott, and C. Deser, 2000: Processes that influence sea surface temperature and ocean mixed layer depth variability in a coupled model. *J. Geophys. Res.,* **105,** 16 823–16 842.

——, I. Blade, M. Newman, J. R. Lanzante, N.-C. Lau, and J. D. Scott, 2002: The atmospheric bridge. The influence of ENSO teleconnections on air–sea interaction over the global oceans. *J. Climate,* **15,** 2205–2231.

Barsugli, J. J., 1995: Idealized models of intrinsic midlatitude atmosphere–ocean interaction. Ph.D. thesis, University of Washington, 187 pp. [Available online at http://www.cdc.noaa.gov/~jjb/thesis.html.]

——, and D. S. Battisti, 1998: The basic effects of atmosphere–ocean thermal coupling on midlatitude variability. *J. Atmos. Sci.,* **55,** 477–493.

Bhatt, U. S., M. A. Alexander, D. S. Battisti, D. D. Houghton, and L. M. Keller, 1998: Atmosphere–ocean interaction in the North Atlantic: Near-surface climate variability. *J. Climate,* **11,** 1615–1632.

Blade, I., 1997: The influence of midlatitude coupling on the low frequency variability of a GCM. Part I: No tropical SST forcing. *J. Climate,* **10,** 2087–2106.

Cayan, D. R., 1992: Latent and sensible heat flux anomalies over the northern oceans: Driving the sea surface temperature. *J. Phys. Oceanogr.,* **22,** 859–881.

Davis, R. E., 1976: Predictability of sea surface temperature and sea level pressure anomalies over the North Pacific Ocean. *J. Phys. Oceanogr.,* **6,** 249–266.

De Coetlogon, G., and C. Frankignoul, 2003: On the persistence of winter sea surface temperature in the North Atlantic. *J. Climate,* in press.

Derber, J., and A. Rosati, 1989: A global oceanic data assimilation system. *J. Phys. Oceanogr.,* **19,** 1333–1347.

Deser, C., and M. S. Timlin, 1997: Atmosphere–ocean interaction on weekly timescales in the North Atlantic and Pacific. *J. Climate,* **10,** 393–408.

Frankignoul, C., 1985: Sea surface temperature anomalies, planetary waves and air–sea feedback in middle latitudes. *Rev. Geophys.,* **23,** 357–390.

——, and K. Hasselmann, 1977: Stochastic climate models. Part 2. Application to sea-surface temperature variability and thermocline variability. *Tellus,* **29,** 289–305.

——, and R. W. Reynolds, 1983: Testing a dynamical model for midlatitude sea surface temperature anomalies. *J. Phys. Oceanogr.,* **13,** 1131–1145.

——, A. Czaja, and B. L'Heveder, 1998: Air–sea feedback in the North Atlantic and surface boundary conditions for ocean models. *J. Climate,* **11,** 2310–2324.

Gaspar, P., 1988: Modeling the seasonal cycle of the upper ocean. *J. Phys. Oceanogr.,* **18,** 161–180.

Hall, A., and S. Manabe, 1997: Can local linear stochastic theory explain sea surface temperature and salinity variability? *Climate Dyn.,* **13,** 167–180.

Haney, R. L., 1985: Midlatitude sea surface temperature anomalies: A numerical hindcast. *J. Phys. Oceanogr.,* **15,** 787–799.

Herterich, K., and K. Hasselmann, 1987: Extraction of mixed layer advection velocities, diffusion coefficients, feedback factors and atmospheric forcing parameters from the statistical analysis of North Pacific SST anomaly fields. *J. Phys. Oceanogr.,* **17,** 2145–2156.

Kushnir, Y., W. A. Robinson, I. Blade, N. M. J. Hall, S. Pend, and R. Sutton, 2002: Atmospheric GCM response to extratropical SST anomalies: Synthesis and evaluation. *J. Climate,* **15,** 2233–2256.

Lagerloef, G. S. E., 1995: Interdecadal variations in the Alaska gyre. *J. Phys. Oceanogr.,* **25,** 2242–2258.

Lau, N.-C., and M. J. Nath, 1996: The role of the ''atmospheric bridge'' in linking tropical Pacific ENSO events to extratropical SST anomalies. *J. Climate,* **9,** 2036–2057.

Levitus, S., and T. P. Boyer, 1994: *Temperature.* Vol. 4, *World Ocean Atlas 1994,* NOAA Atlas NESDIS 4, 117 pp.

Manabe, S., and R. J. Stouffer, 1988: Two stable equilibria of a coupled ocean–atmosphere model. *J. Climate,* **1,** 841–866.

Miller, A. J., W. B. White, and D. R. Cayan, 1997: North Pacific thermocline variations on ENSO timescales. *J. Phys. Oceanogr.,* **27,** 2023–2039.

Monterey, G. I., and S. Levitus, 1997: Climatological cycle of mixed layer depth in the World Ocean. NOAA NESDIS, 92 pp.

Namias, J., and R. M. Born, 1970: Temporal coherence in North Pacific sea-surface temperature patterns. *J. Geophys. Res.,* **75,** 5952–5955.

——, and ——, 1974: Further studies of temporal coherence in North Pacific sea surface temperatures. *J. Geophys. Res.,* **79,** 797–798.

——, X. Yuan, and D. R. Cayan, 1988: Persistence of North Pacific sea surface temperature and atmospheric flow patterns. *J. Climate,* **1,** 682–703.

Peng, S. L., W. A. Robinson, and M. P. Hoerling, 1997: The modeled atmospheric response to midlatitude SST anomalies and its dependence upon background circulation states. *J. Climate,* **10,** 971–987.

Pierce, D. W., T. P. Barnett, N. Schneider, R. Saravanan, D. Dommenget, and M. Latif, 2001: The role of ocean dynamics in producing decadal climate variability in the North Pacific. *Climate Dyn.,* **18,** 51–70.

Qiu, B., 2002: The Kuroshio Extension System: Its large-scale variability and role in the midlatitude ocean–atmosphere interaction. *Japan. J. Oceanogr.,* **58,** 57–75.

Raynor, N. A., E. B. Horton, D. E. Parker, C. K. Folland, and R. B. Hackett, 1996: Version 2.3 of the global sea ice and sea surface temperature data set 1903–1994. CRTN 74. [Available from Hadley Centre for Climate Prediction and Research, London Rd., Bracknell, Berkshire RG12 2SY, United Kingdom.]

Reynolds, R. W., 1978: Sea surface temperature anomalies in the North Pacific Ocean. *Tellus,* **30,** 97–103.

Schneider, N., and A. J. Miller, 2001: Predicting western North Pacific Ocean climate. *J. Climate,* **14,** 3997–4002.

Seager, R., Y. Kushnir, and M. A. Cane, 1995: On heat flux boundary conditions for ocean models. *J. Phys. Oceanogr.,* **25,** 3219–3230.

——, ——, M. Visbeck, N. Naik, J. Miller, G. Krahmann, and H. Cullen, 2000: Causes of Atlantic Ocean climate variability between 1958 and 1998. *J. Climate,* **13,** 2845–2862.

——, ——, ——, ——, M. Cane, and J. Miller, 2001: Wind-driven shifts in the latitude of the Kuroshio–Oyashio Extension and generation of SST anomalies on decadal timescales. *J. Climate,* **14,** 4249–4265.

Timlin, M. S., M. A. Alexander, and C. Deser, 2002: On the reemergence of North Atlantic SST anomalies. *J. Climate,* **15,** 2707–2712.

Watanabe, M., and M. Kimoto, 2000: On the persistence of decadal SST anomalies in the North Atlantic. *J. Climate,* **13,** 3017–3028.

White, W. B., 1995: Design of a global observing system for gyre-scale upper ocean temperature variability. *Progress in Oceanography,* Vol. 36, Pergamon, 169–217.

Woodruff, S. D., R. J. Slutz, R. L. Jenne, and P. M. Steurer, 1987: A Comprehensive Ocean–Atmosphere Data Set. *Bull. Amer. Meteor. Soc.,* **68,** 1239–1250.